Journal of Materials Chemistry A

ROYAL SOCIETY OF CHEMISTRY

PAPER

View Article Online
View Journal | View Issue

Cite this: *J. Mater. Chem. A*, 2020, **8**, 4362

Perovskite-supported Pt single atoms for methane activation

Qiang Wan,[ab] Victor Fung,[c] Sen Lin,[b] Zili Wu[cd] and De-en Jiang*[a]

Received 24th October 2019
Accepted 13th January 2020

DOI: 10.1039/c9ta11712a

rsc.li/materials-a

ABO_3 perovskites are increasingly being explored as catalysts, but it is unclear how they behave as supports for single atoms and how the subsequent single-atom catalysts can be employed for important reactions such as methane activation. Here we examine the stability of Pt single atoms (Pt_1) on the commonly exposed (100) surfaces of $SrBO_3$ perovskites (B = 3d transition metals) and their methane-adsorption properties by first principles density functional theory. We find that the stability and charge state of Pt_1 on the $SrBO_3$(100) surfaces are termination-sensitive. Due to polar compensation, Pt_1 is negatively charged on the A termination but positively charged on the B termination. This charge state greatly impacts methane adsorption: negatively charged Pt_1 on the A-termination chemisorbs methane (in some cases, dissociatively), but positively charged Pt_1 on the B-termination adsorbs methane physically. Analysis of the density of states of the negatively charged Pt_1 reveals that its sp states are key to methane chemisorption and C–H activation. Our work shows that polar compensation on the perovskite surfaces can be used to tune the charge state of a single atom for methane chemisorption and C–H activation.

1. Introduction

Single-atom catalysts (SACs) are a prominent class of heterogeneous catalysts due to their unique activity and atomic efficiency.[1–3] In most cases, noble-metal atoms are atomically dispersed on an oxide support, such as Pt_1 on CeO_2.[4–6] SACs also include surface-dispersed mononuclear organometallic catalysts,[7] micropore-confined single atom catalysts,[8] and atomically dispersed metal atoms on a metal surface[9] or a nanoparticle.[10] Moreover, SACs have also been increasingly used for electrocatalysis[11] and in organic chemistry.[12]

The most studied oxide supports for SACS are binary oxides including FeO_x, Al_2O_3, TiO_2 and CeO_2.[4,13–15] A great deal of efforts have been devoted to understanding the interaction between single atoms and oxide supports, to avoid sintering of the single atoms into larger particles.[16–19] On the other hand, more complex oxides have been explored as supports to tune the interactions.[20–22]

Perovskites (ABO_3) are the most common type of ternary oxides.[23,24] The great variability in choices of A and B serves as an ideal test ground for probing their interactions with a single atom.[25,26] Recently, there has been great interest in using perovskites for catalysis and understanding the structure–activity–selectivity relationships for various facets and terminations of perovskites.[27–29]

CH_4 activation and conversion on SACs have attracted interest lately.[30–32] For example, it was reported that Pt/Cu(111) single-atom alloys can activate C–H bonds while efficiently preventing coke formation.[33] Density functional theory (DFT) predicted that single atoms such as Ir_1 and Pt_1 substitutionally doped on the (110) surface of rutile oxides can chemisorb methane, leading to a facile C–H activation.[34,35]

From the perspective of CH_4 adsorption and activation on SACs, we think that a great opportunity exists in exploring how single atoms interact with perovskites and how the resulting SACs adsorb and activate methane. Hence, herein we use Pt_1 as a prototypical single atom and Sr-based perovskite ($SrBO_3$) as the support, to examine from first principles the effect of varying B ions on the interaction between Pt_1 and $SrBO_3$ and the subsequent impact on CH_4 adsorption and activation. Below we first describe the DFT method employed.

2. Computational method

The Vienna *Ab Initio* simulation package (VASP) was used to perform spin-polarized density functional theory calculations in the generalized-gradient approximation (GGA) with the Perdew–Burke–Ernzerhof (PBE) functional.[36–38] (Here we did not employ any dispersion correction, so that we could clearly distinguish chemisorption and physisorption of methane, a strategy employed previously;[34] including the dispersion correction did not change our conclusions.) Electronic wave functions were expanded in plane waves with a cutoff energy of 450 eV and the

[a]*Department of Chemistry, University of California, Riverside, California 92521, USA. E-mail: djiang@ucr.edu*

[b]*State Key Laboratory of Photocatalysis on Energy and Environment, College of Chemistry, Fuzhou University, Fuzhou 350002, China*

[c]*Center for Nanophase Materials Sciences, Oak Ridge National Laboratory, Oak Ridge, Tennessee 37831, USA*

[d]*Chemical Sciences Division, Oak Ridge National Laboratory, Oak Ridge, Tennessee 37831, USA*

core electrons with the nucleus were approximated by the projector augmented-wave (PAW) method.[39] The convergence criteria were 10^{-4} eV and 0.01 eV $Å^{-1}$ for energy and force, respectively.

As in previously pursued strategies,[25,26,29] we focus on the two main terminations of the $SrBO_3(100)$ surface, one of the most stable and commonly exposed surfaces. The (100) facet of $SrBO_3$ in either A- or B-termination was modelled as a 2×2 supercell with a vacuum space of 15 Å along the z direction. The surface slabs have six layers, with the bottom four layers fixed in their bulk positions, and were sampled using a $3 \times 3 \times 1$ k-point mesh in the Monkhorst–Pack scheme.[40] The interaction of Pt_1 with the surface was determined by the Pt_1 adsorption energy

$$E_{\text{ads-Pt}_1} = E_{\text{Pt}_1\text{-ABO}_3} - E_{\text{Pt}_1} - E_{\text{ABO}_3},$$

where $E_{\text{Pt}_1\text{-ABO}_3}$, E_{Pt_1} and E_{ABO_3} represent the energies of the ABO_3-supported Pt_1 single-atom catalyst, a Pt atom in the gas phase, and the ABO_3 surface, respectively. The same approach was used to compute methane adsorption energy on ABO_3-supported Pt_1 single-atom catalysts. O vacancy formation energy ($E_{\text{O-VFE}}$) was calculated with the following equation:

$$E_{\text{O-VFE}} = E_{\text{defect-ABO}_3} - \frac{1}{2}E_{\text{O}_2} - E_{\text{ABO}_3},$$

where $E_{\text{defect-ABO}_3}$ and E_{O_2} represent the calculated energies of the ABO_3 surface with an O vacancy and a gas phase O_2 molecule, respectively.

The charge-density difference was calculated with the following equation:

$$\Delta\rho = \rho_{\text{Pt}_1\text{-SrTiO}_3} - \rho_{\text{SrTiO}_3} - \rho_{\text{Pt}_1},$$

where $\rho_{\text{Pt}_1\text{-SrTiO}_3}$, ρ_{SrTiO_3} and ρ_{Pt_1} represent the calculated electron densities of Pt_1-$SrTiO_3$, $SrTiO_3$, and Pt_1, respectively.

3. Results and discussion

Sr-based perovskites have been widely studied,[25] so we chose Sr^{2+} as the A cation in this work. We vary the B cation in $SrBO_3$ in 3d transition metals (B = Ti, V, Cr, Mn, Fe, Co, Ni, Cu). The (100) facets are usually the most stable facets of perovskite (ABO_3).[41,42] In this $SrBO_3(100)$ system, we first study the adsorption of the Pt single atom on the $SrBO_3(100)$ surface to evaluate the interaction between Pt_1 and perovskite oxides.

3.1. Adsorption of Pt single atom on $SrBO_3(100)$

The $SrBO_3(100)$ facet can have either the A- or B-termination. The A-termination exposes the SrO layer (Fig. 1a) while the B-termination exposes the BO_2 layer (Fig. 1b). On A-termination, we found that Pt_1 prefers to locate at the top of a surface oxygen atom (Fig. 1c), while on B-termination, Pt_1 is most stable at the hollow site and coordinated by four O (Fig. 1d).

The Pt_1 adsorption energies (relative to a gas-phase Pt atom) on the two $SrBO_3(100)$ terminations with varying B are plotted in Fig. 2. Interestingly, one can see that on A-termination, Pt_1 adsorption energy is relatively constant, fluctuating slightly around −3.0 eV, with varying B cations. In contrast, the Pt_1 adsorption energy on the B-termination increases in magnitude from −3.09 eV on $SrTiO_3(100)$ to −9.22 eV on $SrCuO_3(100)$. Apparently, the changing B ion has a much greater impact for Pt_1 interaction on the B-termination than on the A-termination. This is consistent with the difference in the Pt_1 adsorption geometry on the two terminations (Fig. 1c and d): the formation of 4 Pt–O bonds in the B-termination suggests that the Pt adsorption on the B termination will be much more impacted by the B ion. Below we further examine this difference by correlating with descriptors that vary with the B ion.

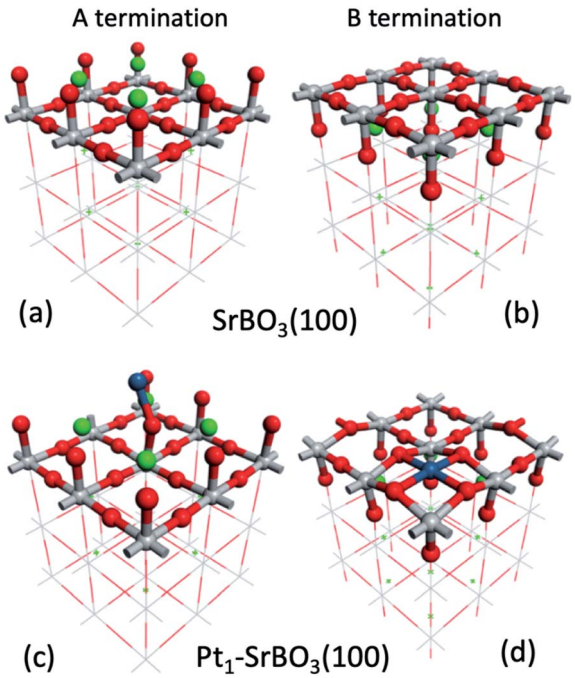

Fig. 1 Typical structures of $SrBO_3(100)$ and Pt_1-$SrBO_3(100)$: (a) $SrBO_3(100)$ A-termination; (b) $SrBO_3(100)$ B-termination; (c) Pt_1 on $SrBO_3(100)$ A-termination; (d) Pt_1 on $SrBO_3(100)$ B-termination. Color code: O, red; Sr, green; B, gray; Pt, blue.

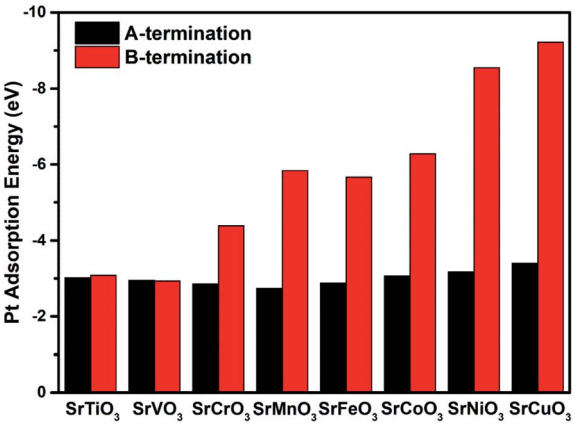

Fig. 2 Adsorption energies of Pt single atom on $SrBO_3(100)$ surfaces, for B = Ti, V, Cr, Mn, Fe, Co, Ni, Cu.

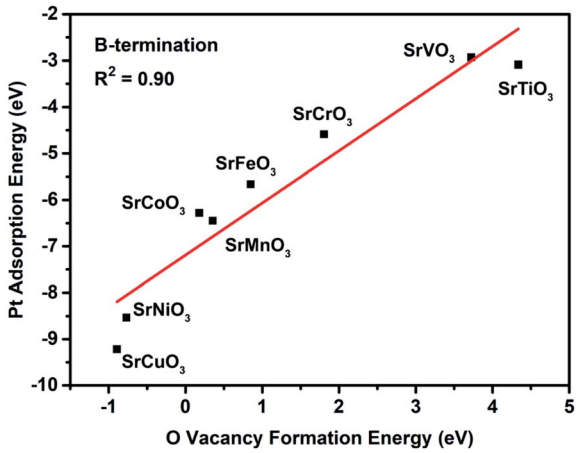

Fig. 3 Correlation between Pt single atom adsorption energy and surface O vacancy formation energy on $SrBO_3$(100) B termination. The red line represents the best linear fit.

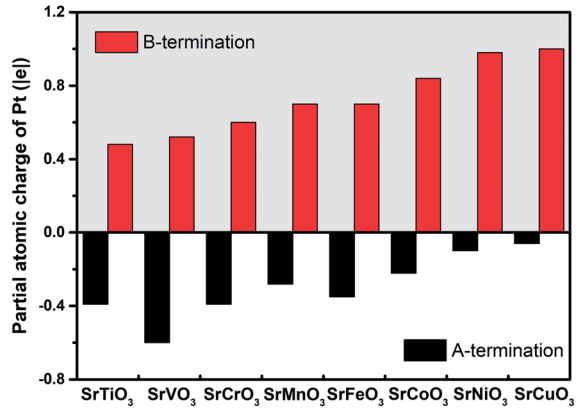

Fig. 4 Partial atomic charge of Pt single atom on $SrBO_3$(100).

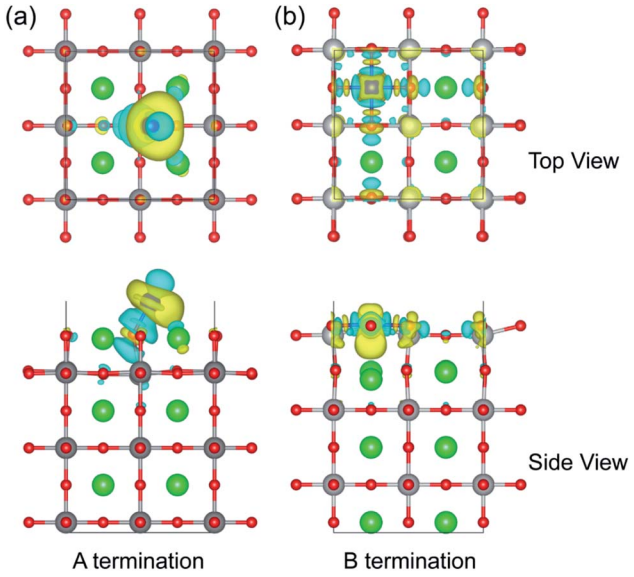

Fig. 5 Charge-density difference plots of Pt_1-$SrTiO_3$(100): (a) A-termination; (b) B-termination. Blue denotes depletion of electron density while yellow represents accumulation. Color code: O, red; Sr, green; Ti, gray. Pt_1 is at the center of the charge transfer. The isosurface value is equal to 0.0038 e $Å^{-3}$.

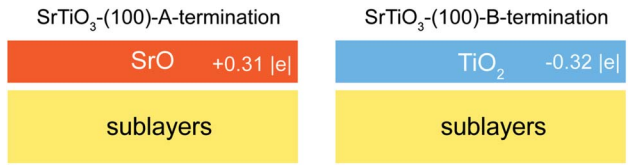

Fig. 6 Charge of surface layers on $SrTiO_3$(100) for A-termination and B-termination. The surface-layer charge is determined by the sum of the Bader charges of all the atoms in the top layer of the surface before Pt_1 adsorption (Table 1).

3.2. Correlation with the vacancy formation energy

Commonly used descriptors for oxides and perovskites in terms of their surface reactivity include O-vacancy formation energy (O-VFE), H adsorption energy, and surface-oxygen Bader charges.[19,43,44] To understand the trend of Pt adsorption on the B-termination (Fig. 2), we calculated surface O-VFE of the $SrBO_3$(100) B terminations. As one can see from Fig. 3, the O-VFE correlates well with Pt adsorption energy. In other words, as B changes from Ti to Cu, the surface becomes more reducible and the surface O becomes more reactive, leading to stronger interaction with Pt on the surface.

Table 1 Bader charges (in |e|) of Pt_1, O atoms bound to Pt_1, and nearest A and B ions to Pt_1 on the surface after/before Pt adsorption on the A- and B-terminations of $SrBO_3$(100)

	A-Termination			B-Termination		
B in $SrBO_3$	Pt_1	O	Sr	Pt_1	O	B
Ti	−0.39/0.00	−1.04/−1.27	1.57/1.58	0.48/0.00	−1.01/−1.11	1.85/1.91
V	−0.60/0.00	−1.02/−1.25	1.57/1.57	0.52/0.00	−1.00/−1.05	1.73/1.77
Cr	−0.39/0.00	−1.02/−1.21	1.56/1.57	0.60/0.00	−0.96/−0.99	1.66/1.71
Mn	−0.28/0.00	−0.95/−1.18	1.56/1.57	0.70/0.00	−0.91/−0.95	1.60/1.65
Fe	−0.35/0.00	−0.97/−1.30	1.57/1.62	0.70/0.00	−0.92/−0.94	1.50/1.53
Co	−0.22/0.00	−0.94/−1.16	1.56/1.56	0.84/0.00	−0.86/−0.83	1.32/1.37
Ni	−0.10/0.00	−0.81/−1.10	1.57/1.57	0.98/0.00	−0.79/−0.78	1.19/1.24
Cu	−0.06/0.00	−0.78/−1.10	1.57/1.57	1.00/0.00	−0.78/−0.77	1.15/1.17

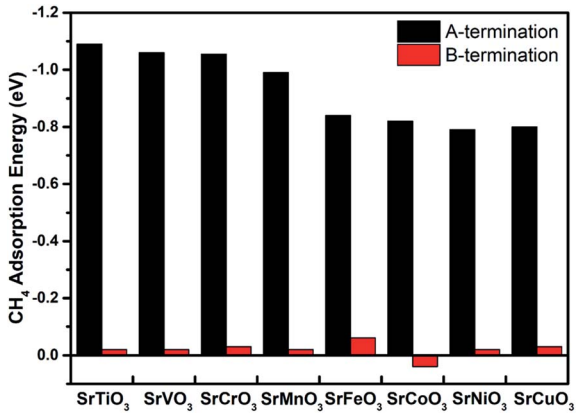

Fig. 7 CH_4 adsorption energy on Pt_1-$SrBO_3$(100).

3.3. Charge and distribution on and around Pt_1 supported by $SrBO_3$(100)

Since the charge state is an important indicator of the reactivity of a single atom site, we have examined the Bader charge of the Pt single atom on $SrBO_3$(100) in preparation for examining their methane-adsorbing ability.[45] Interestingly, Fig. 4 shows that Pt atoms are negatively charged on the A-termination but positively charged on the B-termination (Bader charges of other surface atoms after and before Pt adsorption are shown in Table 1). When B cation changes from Ti to Cu, the Pt charge increases: becoming more positive on the B termination and less negative on the A termination.

To pinpoint how the electron transfers between Pt single atom and the surface, we use $SrTiO_3$(100) as an example and analyzed the charge-density difference after supporting the Pt single atom. As one can see from Fig. 5, Pt gains electrons from the O atom underneath and becomes negatively charged on the A-termination (Fig. 5a), but on the B-termination, the charge transfer is more complex (Fig. 5b) and overall Pt_1 loses some electron density while Ti gains (Table 1).

The different charges of Pt_1 on A- and B-terminations of $SrBO_3$(100) can be understood by polar compensation.[46–51] Using $SrTiO_3$(100) as an example, Fig. 6 shows that the A-termination is slightly positively charged, while the B-termination is negatively charged. This is in agreement with previous theoretical findings that the $SrTiO_3$(100) surfaces are slightly polar.[52] To compensate the surface charges, Pt_1 should have negative charge on the A-

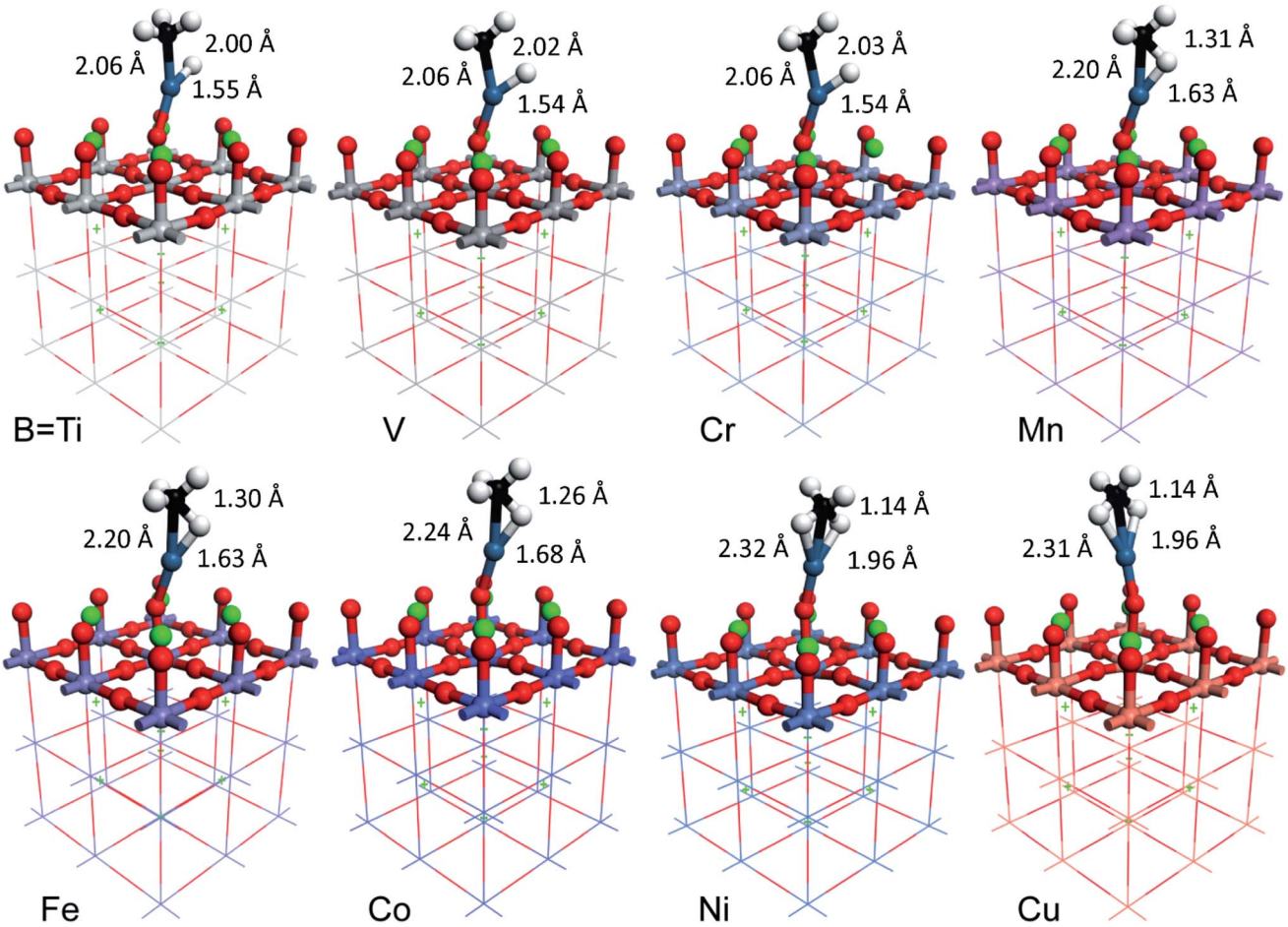

Fig. 8 Optimized geometry of CH_4 adsorption on Pt_1-$SrBO_3$(100) A-termination. Color code: O, red; Sr, green; Pt, blue; C, black; H, white; B, varies. Key bond distances are also given for the C–H bond being activated: Pt–C (left), Pt–H (lower right), and C–H (upper right).

termination and positive charge on the B-termination. That is exactly what we have found from Fig. 4.

3.4. CH_4 adsorption on Pt_1-$SrBO_3$(100)

We next examine CH_4 adsorption on Pt_1-$SrBO_3$(100). Fig. 7 shows that on the B-termination, adsorption of CH_4 on Pt_1-$SrBO_3$(100) is physical in nature and weak, but on the A-termination, CH_4 chemisorbs strongly with adsorption energies in the range of −0.8 to −1.1 eV. To understand this strong adsorption, we further inspected the optimized geometry of the adsorbed CH_4. As shown in Fig. 8, for B being the early transition metals, such as in $SrTiO_3$, $SrVO_3$ and $SrCrO_3$, dissociative adsorption happens, leading to co-adsorbed H and CH_3 on Pt_1. For B = Mn to Cu, one or two C–H bonds of CH_4 are significantly activated and elongated, though not broken, in the chemisorbed state (Fig. 8).

The spontaneous CH_4 dissociation that we found on systems such as Pt_1-$SrTiO_3$-(100)-A-termination is consistent with several recent studies of CH_4 activation by gas phase atoms or clusters. For example, Perera *et al.*[53] found that the insertion of a gas-phase Pt atom into the C–H bond of CH_4 is barrierless to form CH_3–Pt–H, based on a joint vacuum ultraviolet photoionization and DFT investigation. More relevantly, Zhao *et al.* found from mass spectrometry and DFT calculations that small gas-phase anionic clusters such as $PtAl_2O_4^-$ and $AuTi_3O_7^-$ can activate CH_4.[54,55]

To understand why CH_4 adsorbs strongly on Pt_1-$SrBO_3$(100) A-termination, we plotted the local density of states (DOS) of Pt_1 on $SrTiO_3$(100) (similar results have been found for other strong-interaction cases such as B = V and Cr). As one can see, there are empty 6s and 6p states (especially p_z) of Pt_1 right above the Fermi level (Fig. 9a and b). These states serve as an acceptor for σ donation from the C–H bond of CH_4 and have much greater change after adsorption. As revealed previously,[34,35] the key to methane chemisorption from the d states is the empty d_{z^2} orbital, but it is occupied in the case of Pt_1-$SrTiO_3$-(100)-A (Fig. 9c). Hence, the empty sp states on Pt_1-$SrBO_3$-(100)-A play the dominant role in methane chemisorption. In contrast, the weak methane chemisorption on Pt_1-$SrTiO_3$-(100)-B (Fig. 7) can be attributed to the lack of either empty sp states (Fig. 10a) or empty d_{z^2} states near the Fermi level (Fig. 10b).

3.5. Implications for methane activation

Considering both the stability (Fig. 2) and methane adsorption (Fig. 7), one can see that the A terminations of $SrTiO_3$(100) and $SrVO_3$(100) are most promising to realize methane

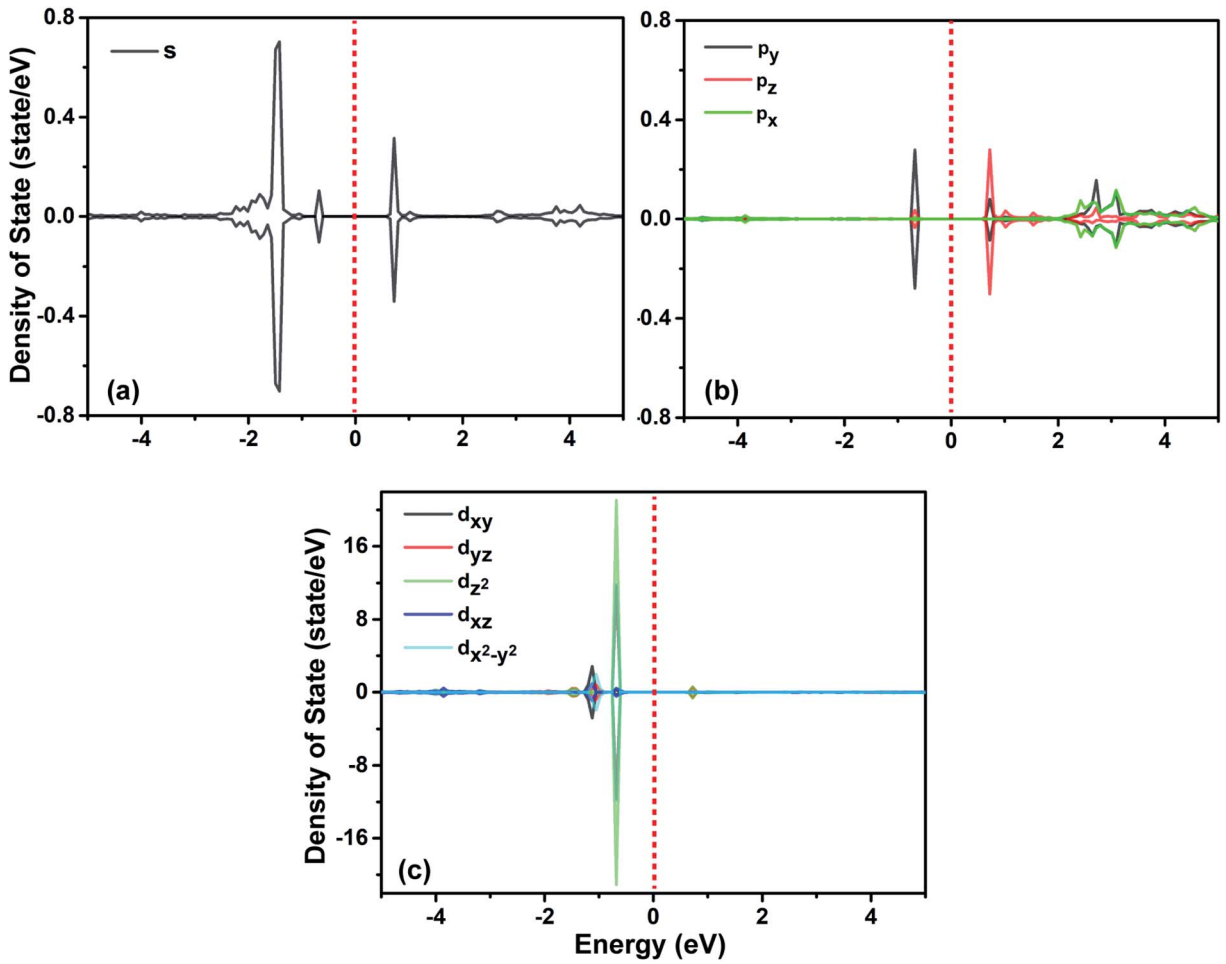

Fig. 9 Projected density of states of Pt single atom on $SrTiO_3$(100) A-termination before CH_4 adsorption: (a) 6s states; (b) 6p states; (c) 5d states. The Fermi level is set to 0 eV.

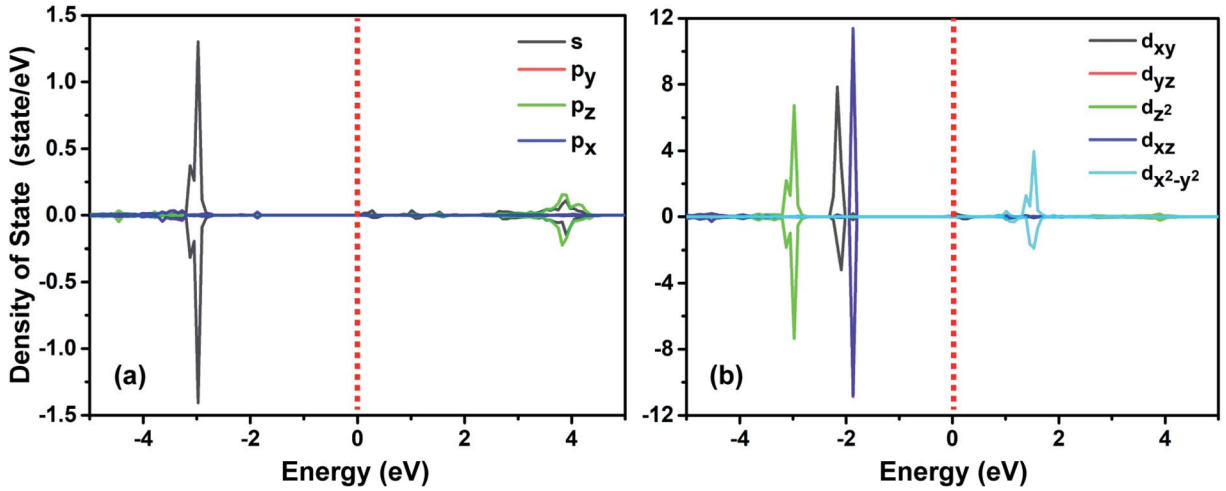

Fig. 10 Projected density of states of Pt single atom on $SrTiO_3$(100) B-termination before CH_4 adsorption. (a) s, p states; (b) d states. The Fermi level is set to 0 eV.

chemisorption and facile activation at the Pt_1 site, because Pt_1 has about equal stability on the A and B terminations of those two surfaces. For the (100) surfaces of the other perovskites explored, Pt_1 strongly prefers the B termination where methane only physisorbs at the Pt_1 site; but as shown previously,[24] the perovskite surfaces can reconstruct at various pretreatment methods and under certain conditions the A termination can be exposed. In this case, Pt_1 can be anchored on the A termination to test methane activation. Fig. 2 shows that the adsorption energy of Pt_1 on the A terminations is about −3.0 eV relative to a gas-phase Pt atom, while bulk Pt has a cohesive energy of 5.5 eV per atom from our DFT calculation. This means that Pt_1 on the A terminations is much less stable than bulk Pt and may sinter at high temperatures, which brings challenges in synthesis. On the other hand, Pt_1 may be kinetically stabilized on the A termination. We have investigated minimum-energy diffusion pathways of Pt_1 on the A- and B-terminations of $SrTiO_3$(100), as an example. We found that the diffusion barrier is actually higher on the A-termination ($E_a = 1.37$ eV) that on the B-termination ($E_a = 1.18$ eV).

4. Conclusions

In summary, we have studied methane adsorption on the Pt single atom stabilized on the (100) surfaces of $SrBO_3$ perovskites (B = 3d transition metals) by first principles density functional theory. We found that as B varies from Ti to Cu, the binding energy of Pt_1 with the A (or SrO) termination is about the same, but the binding of Pt_1 with the B (or BO_2) termination becomes stronger which correlates with the increasing reducibility as measured by the oxygen-vacancy formation energy. More interestingly, Pt_1 is negatively charged on the A termination but positively charged on the B termination, due to polar compensation. This charge state has a profound impact on methane adsorption: methane adsorbs strongly, chemically, and, in some cases, dissociatively on Pt_1-$SrBO_3$(100)-A-termination, but weakly and physically on Pt_1-$SrBO_3$(100)-B-termination. Analysis of the local density of states revealed that the sp states of the negatively charged Pt_1 are key to methane chemisorption and C–H activation. Our work shows that negatively charged Pt_1 single atoms on the A termination of the $SrBO_3$(100) have the potential to achieve facile C–H activation of methane.

Conflicts of interest

There are no conflicts to declare.

Acknowledgements

This work was sponsored by the U.S. Department of Energy, Office of Science, Office of Basic Energy Sciences, Chemical Sciences, Geosciences, and Biosciences Division, Catalysis Science Program. This research used resources of the National Energy Research Scientific Computing Center, a DOE Office of Science User Facility supported by the Office of Science of the U.S. Department of Energy under contract no. DE-AC02-05CH11231.

References

1 X.-F. Yang, A. Wang, B. Qiao, J. Li, J. Liu and T. Zhang, *Acc. Chem. Res.*, 2013, **46**, 1740–1748.
2 Y. Tang, Y. Li, V. Fung, D. E. Jiang, W. Huang, S. Zhang, Y. Iwasawa, T. Sakata, L. Nguyen, X. Zhang, A. I. Frenkel and F. F. Tao, *Nat. Commun.*, 2018, **9**, 1231.
3 J. Lin, B. Qiao, J. Liu, Y. Huang, A. Wang, L. Li, W. Zhang, L. F. Allard, X. Wang and T. Zhang, *Angew. Chem., Int. Ed.*, 2012, **51**, 2920–2924.
4 L. Nie, D. Mei, H. Xiong, B. Peng, Z. Ren, X. I. P. Hernandez, A. DeLaRiva, M. Wang, M. H. Engelhard, L. Kovarik, A. K. Datye and Y. Wang, *Science*, 2017, **358**, 1419.
5 F. Dvorak, M. Farnesi Camellone, A. Tovt, N. D. Tran, F. R. Negreiros, M. Vorokhta, T. Skala, I. Matolinova, J. Myslivecek, V. Matolin and S. Fabris, *Nat. Commun.*, 2016, **7**, 10801.
6 Y. Tang, Y.-G. Wang and J. Li, *J. Phys. Chem. C*, 2017, **121**, 11281–11289.

7 J. M. Thomas, R. Raja and D. W. Lewis, *Angew. Chem., Int. Ed.*, 2005, **44**, 6456–6482.
8 P.-P. Knops-Gerrits, D. De Vos, F. Thibault-Starzyk and P. A. Jacobs, *Nature*, 1994, **369**, 543–546.
9 G. Kyriakou, M. B. Boucher, A. D. Jewell, E. A. Lewis, T. J. Lawton, A. E. Baber, H. L. Tierney, M. Flytzani-Stephanopoulos and E. C. H. Sykes, *Science*, 2012, **335**, 1209.
10 H. Li, W. Chai and G. Henkelman, *J. Mater. Chem. A*, 2019, **7**, 23868–23877.
11 J. Su, R. Ge, Y. Dong, F. Hao and L. Chen, *J. Mater. Chem. A*, 2018, **6**, 14025–14042.
12 H. Yan, C. Su, J. He and W. Chen, *J. Mater. Chem. A*, 2018, **6**, 8793–8814.
13 B. Qiao, A. Wang, X. Yang, L. F. Allard, Z. Jiang, Y. Cui, J. Liu, J. Li and T. Zhang, *Nat. Chem.*, 2011, **3**, 634–641.
14 J. H. Kwak, J. Hu, D. Mei, C.-W. Yi, D. H. Kim, C. H. F. Peden, L. F. Allard and J. Szanyi, *Science*, 2009, **325**, 1670.
15 L. DeRita, J. Resasco, S. Dai, A. Boubnov, H. V. Thang, A. S. Hoffman, I. Ro, G. W. Graham, S. R. Bare, G. Pacchioni, X. Pan and P. Christopher, *Nat. Mater.*, 2019, **18**, 746–751.
16 Y.-Q. Su, Y. Wang, J.-X. Liu, I. A. W. Filot, K. Alexopoulos, L. Zhang, V. Muravev, B. Zijlstra, D. G. Vlachos and E. J. M. Hensen, *ACS Catal.*, 2019, **9**, 3289–3297.
17 Y. Q. Su, J. X. Liu, I. A. W. Filot and E. J. M. Hensen, *Chem. Mater.*, 2017, **29**, 9456–9462.
18 Q. Wan, F. Wei, Y. Wang, F. Wang, L. Zhou, S. Lin, D. Xie and H. Guo, *Nanoscale*, 2018, **10**, 17893–17901.
19 N. J. O'Connor, A. S. M. Jonayat, M. J. Janik and T. P. Senftle, *Nat. Catal.*, 2018, **1**, 531–539.
20 R. Lang, W. Xi, J. C. Liu, Y. T. Cui, T. Li, A. F. Lee, F. Chen, Y. Chen, L. Li, L. Li, J. Lin, S. Miao, X. Liu, A. Q. Wang, X. Wang, J. Luo, B. Qiao, J. Li and T. Zhang, *Nat. Commun.*, 2019, **10**, 234.
21 S. Dong, Y. Zhang, X. Zhang, J. Mao and Z. Yang, *J. Phys. Chem. C*, 2018, **122**, 1622–1630.
22 J. Zhang, X. Wu, W. C. Cheong, W. Chen, R. Lin, J. Li, L. Zheng, W. Yan, L. Gu, C. Chen, Q. Peng, D. Wang and Y. Li, *Nat. Commun.*, 2018, **9**, 1002.
23 J. Hwang, R. R. Rao, L. Giordano, Y. Katayama, Y. Yu and Y. Shao-Horn, *Science*, 2017, **358**, 751.
24 B. Madhavan and A. Ashok, *Ionics*, 2014, **21**, 601–610.
25 V. Fung, Z. Wu and D. E. Jiang, *J. Phys. Chem. Lett.*, 2018, **9**, 6321–6325.
26 V. Fung, F. Polo-Garzon, Z. Wu and D.-e. Jiang, *Catal. Sci. Technol.*, 2018, **8**, 702–709.
27 F. Polo-Garzon, S. Z. Yang, V. Fung, G. S. Foo, E. E. Bickel, M. F. Chisholm, D. E. Jiang and Z. Wu, *Angew. Chem., Int. Ed.*, 2017, **56**, 9820–9824.
28 F. Polo-Garzon, V. Fung, X. Liu, Z. D. Hood, E. E. Bickel, L. Bai, H. Tian, G. S. Foo, M. Chi, D.-e. Jiang and Z. Wu, *ACS Catal.*, 2018, **8**, 10306–10315.
29 R. Huang, V. Fung, Y. Zhang, D. R. Mullins, Z. Wu and D.-e. Jiang, *J. Phys. Chem. C*, 2018, **122**, 7210–7216.
30 X. Guo, G. Fang, G. Li, H. Ma, H. Fan, L. Yu, C. Ma, X. Wu, D. Deng, M. Wei, D. Tan, R. Si, S. Zhang, J. Li, L. Sun, Z. Tang, X. Pan and X. Bao, *Science*, 2014, **344**, 616.
31 Y. Kwon, T. Y. Kim, G. Kwon, J. Yi and H. Lee, *J. Am. Chem. Soc.*, 2017, **139**, 17694–17699.
32 W. Huang, S. Zhang, Y. Tang, Y. Li, L. Nguyen, Y. Li, J. Shan, D. Xiao, R. Gagne, A. I. Frenkel and F. F. Tao, *Angew. Chem., Int. Ed.*, 2016, **55**, 13441–13445.
33 M. D. Marcinkowski, M. T. Darby, J. Liu, J. M. Wimble, F. R. Lucci, S. Lee, A. Michaelides, M. Flytzani-Stephanopoulos, M. Stamatakis and E. C. H. Sykes, *Nat. Chem.*, 2018, **10**, 325–332.
34 V. Fung, F. F. Tao and D. E. Jiang, *Phys. Chem. Chem. Phys.*, 2018, **20**, 22909–22914.
35 V. Fung, G. Hu, F. Tao and D.-e. Jiang, *ChemPhysChem*, 2019, **20**, 2217–2220.
36 G. Kresse and J. Furthmüller, *Comput. Mater. Sci.*, 1996, **6**, 15–50.
37 G. Kresse and J. Furthmüller, *Phys. Rev. B: Condens. Matter Mater. Phys.*, 1996, **54**, 11169–11186.
38 J. P. Perdew, K. Burke and M. Ernzerhof, *Phys. Rev. Lett.*, 1996, **77**, 3865–3868.
39 G. Kresse and D. Joubert, *Phys. Rev. B: Condens. Matter Mater. Phys.*, 1999, **59**, 1758–1775.
40 H. J. Monkhorst and J. D. Pack, *Phys. Rev. B: Solid State*, 1976, **13**, 5188–5192.
41 K. Huang, L. Yuan and S. Feng, *Inorg. Chem. Front.*, 2015, **2**, 965–981.
42 F. Bottin, F. Finocchi and C. Noguera, *Phys. Rev. B: Condens. Matter Mater. Phys.*, 2003, **68**, 035418.
43 G. Kumar, S. L. J. Lau, M. D. Krcha and M. J. Janik, *ACS Catal.*, 2016, **6**, 1812–1821.
44 V. Fung, F. F. Tao and D. E. Jiang, *J. Phys. Chem. Lett.*, 2017, **8**, 2206–2211.
45 W. Tang, E. Sanville and G. Henkelman, *J. Phys.: Condens. Matter*, 2009, **21**, 084204.
46 C. Noguera, *J. Phys.: Condens. Matter*, 2000, **12**, R367–R410.
47 J. Goniakowski, F. Finocchi and C. Noguera, *Rep. Prog. Phys.*, 2008, **71**, 016501.
48 Y. Wang, J. Cheng, M. Behtash, W. Tang, J. Luo and K. Yang, *Phys. Chem. Chem. Phys.*, 2018, **20**, 18515–18527.
49 M. Setvin, M. Reticcioli, F. Poelzleitner, J. Hulva, M. Schmid, L. A. Boatner, C. Franchini and U. Diebold, *Science*, 2018, **359**, 572.
50 Z. Wang, A. Loon, A. Subramanian, S. Gerhold, E. McDermott, J. A. Enterkin, M. Hieckel, B. C. Russell, R. J. Green, A. Moewes, J. Guo, P. Blaha, M. R. Castell, U. Diebold and L. D. Marks, *Nano Lett.*, 2016, **16**, 2407–2412.
51 B. E. Gaddy, E. A. Paisley, J.-P. Maria and D. L. Irving, *Phys. Rev. B: Condens. Matter Mater. Phys.*, 2014, **90**, 125403.
52 E. Heifets, R. I. Eglitis, E. A. Kotomin, J. Maier and G. Borstel, *Surf. Sci.*, 2002, **513**, 211–220.
53 M. Perera, R. B. Metz, O. Kostko and M. Ahmed, *Angew. Chem., Int. Ed.*, 2013, **52**, 888–891.
54 Y. X. Zhao, Z. Y. Li, Z. Yuan, X. N. Li and S. G. He, *Angew. Chem., Int. Ed.*, 2014, **53**, 9482–9486.
55 Y. X. Zhao, X. N. Li, Z. Yuan, Q. Y. Liu, Q. Shi and S. G. He, *Chem. Sci.*, 2016, **7**, 4730–4735.

